THE JOURNAL OF PHYSICAL CHEMISTRY C

pubs.acs.org/JPCC

Article

Chemical Switching of the Magnetic Coupling in a MnPc Dimer by Means of Chemisorption and Axial Ligands

Barbara Brena,* Biplab Sanyal, and Heike C. Herper

Cite This: *J. Phys. Chem. C* 2020, 124, 27185−27193

Read Online

ACCESS | Metrics & More | Article Recommendations | Supporting Information

ABSTRACT: We present an *ab initio* density functional theory study of the magnetic properties of manganese phthalocyanine dimers, where we focus on the magnetic coupling between the Mn centers and on how it is affected by external factors like chemisorption or atomic axial ligands. We have studied several different configurations for the gas phase dimers, which resulted in ferromagnetic couplings of different magnitudes. For the bare dimer we find a significant ferromagnetic coupling between the Mn centers, which decreases by about 20% when a H atom is adsorbed on one of the Mn atoms and is reduced to about 7% when a Cl atom is adsorbed. The magnetic coupling is almost fully quenched when the dimer, bare or with the H ligand, is deposited on the ferromagnetic substrate Co(001). Our calculations indicate that the coupling between the two Mn atoms principally occurs via a superexchange interaction along two possible paths within a Mn−N−Mn−N four-atom loop. When these electrons get involved in chemical bonding outside the dimer itself, an appreciable alteration of the overlap between Mn and N molecular orbitals along the loop occurs, and consequently, the magnetic interaction between the Mn centers varies. We show that this is reflected by the electronic structure of the dimer in various configurations and is also visible in the structure of the atomic loop. The chemical tuning of the magnetic coupling is highly relevant for the design of nanodevices like molecular spin valves, where the molecules need to be anchored to a support.

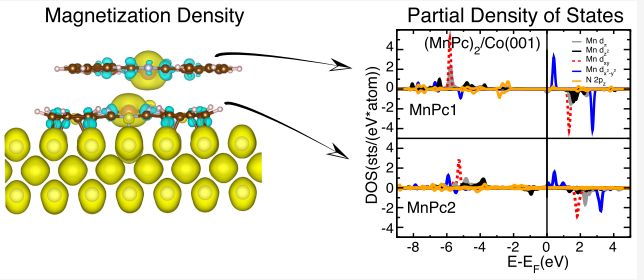

INTRODUCTION

A key objective of molecular electronics and spintronics (spin-based electronics) is the downscaling of the electronic components, which would bring up remarkable benefits like increase in magnetic storage density and reduction of power consumption. In this context, the possibility to use organic molecular materials of low production cost has become highly appealing. The molecules of the phthalocyanine family (Pc) have been studied quite extensively in the emerging field of organic spintronics.[1−4] Among the milestones in this field are the possibility of spin-polarized injection and transport of electrons through organic semiconductors, shown by Dediu and colleagues,[5] and the giant magnetoresistance observed for a single H_2Pc[1] and CoPc.[6] In addition, an organic spin valve device based on immobilized layers of CuPc (spacer layer) and aligned MnPc (or NiPc) as spin-injection and spin-detection layers was fabricated and studied experimentally by Banerjee and co-workers.[7] Recently, also supermolecular nano and low-dimensional structures like molecular chains and dimers have been addressed, with an emphasis on their structures[8] and magnetic properties.[9,10] These systems are promising novel building blocks for molecular size devices as well as model systems to understand the magnetic interactions and spin transfer mechanisms between the molecules or between the molecules and substrates. An important issue in this field is to find feasible mechanisms to manipulate the molecular spin and magnetic moments in a reproducible fashion.

In the present work, we target dimers of the MnPc molecule, which is among the most studied phthalocyanines in molecular spintronics, due to the known magnetic interactions in MnPc-based bulk materials.[11,12] Interestingly, the deposition of MnPc molecules on the ferromagnetic Co(001) surface has shown to generate a so-called *spinterface*,[13,14] i.e., an active heterogeneous interface for spin transport.[3] Beyond that, MnPc and FePc coadsorbed in the form of a checkerboard table on Au(111) were reported to be antiferromagnetically coupled through the Ruderman−Kittel−Kasuya−Yosida (RKKY) exchange interaction via the substrate electronic states.[15] MnPc, shown in Figure 1A, consists of a single Mn center surrounded by an organic ring, representing a sort of archetype of single molecule magnet. The molecule has a spin 3/2 and a D_{2h} symmetry. The magnetic properties of specific phases of MnPc films were described already some decades ago. Both

Received: September 16, 2020
Revised: November 10, 2020
Published: November 24, 2020

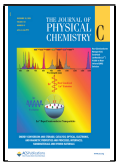

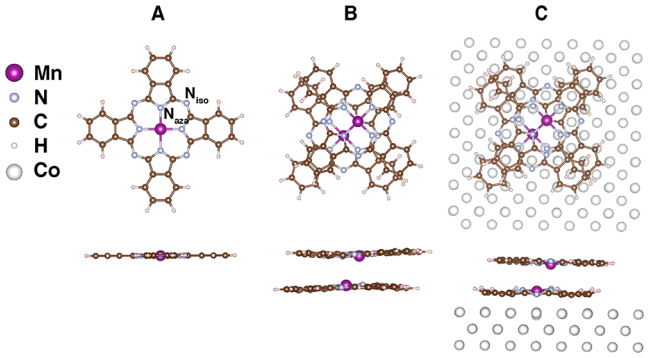

Figure 1. (A) Top view and side view of MnPc, where isoindole N (N_{iso}) and azabridge N (N_{aza}) type atoms are highlighted. (B) Top view and side view of the MnPc dimer in the α+ configuration. (C) Top view and side view of the MnPc dimer in the α+ configuration adsorbed on the Co(001) surface.

ferromagnetic and antiferromagnetic couplings were reported for respectively the β and α phases in bulk MnPc films,[11,12] showing that the magnetic interaction between the molecules is directly linked to their reciprocal arrangement.[12] Because of this, it is essential to unveil how the interplay between the electronic and geometric structure shapes the magnetic properties to engineer the future molecule-scale devices.

We have first studied the magnetic properties of dimers of MnPc in the gas phase, considering several possible molecular configurations by means of *ab initio* density functional theory (DFT) including dispersion interactions. We have then focused on the dimer with the configuration of lowest energy and studied its adsorption on a Co(001) substrate, both bare and with atomic axial ligands such as H and Cl. It has been shown in previous joint theory/experiment studies how these theoretical methods well reproduce the experimental findings for the adsorbate MnPc/Co(100) system in terms of adsorption distances and magnetic properties.[3,16] Previous theoretical studies have reported dimers of phthalocyanines in geometrical configurations that are derived from the various 3D bulk stackings,[8] where the magnetic interactions are directly associated with those in the thick films. We have here analyzed the connection between the magnetic coupling and the inter- and intramolecular chemical bondings that occur in the dimer. The Mn atoms at the center of the molecules are coupled via superexchange interaction, which unrolls via a N atom directly bonded to one of the Mn atoms and situated in the face of the Mn of the opposing molecule, via a mechanism analogous to the one described for MnPc films and bulk materials.[11,12] This type of superexchange path was also experimentally investigated by Chen et al.[17] by means of spin-flip electron tunneling spectroscopy between CoPc molecules adsorbed on a Pb(111) surface, where the CoPc molecules assume a reciprocal configuration analogous to the one of the dimers in our study. We observe that when the Mn atoms take part in intermolecular chemical bonds, the magnetic coupling is markedly reduced. This happens in all cases when the dimer is chemisorbed on a Co surface via one of the MnPc rings or when a H or a Cl atom is axially adsorbed on the Mn center on one side of the dimer. In these cases, the chemical bonding scheme of the Mn atoms is changed, as can be seen in the modifications of the inter- and intramolecular distances between the Mn and N atoms involved.

THEORETICAL METHODS

The present study is based on *ab initio* DFT calculations using the VASP[18] code with the Perdew, Burke, and Ernzerhof (PBE) exchange correlation functional[19,20] and the projector augmented wave method.[21] The plane wave cutoff was 400 eV, and only the Γ-point *k*-mesh was used. An effective Hubbard term U_{eff} of 4 eV was chosen to describe the Mn 3d orbitals, following Dudarev's method.[22] The value for the Hubbard term has been chosen according to the findings in our previous study.[23] This value has been proven to properly reproduce experimental data, for example, photoemission spectra.[23] The long-range dispersion forces were described with Grimme's second method (D2).[24] For comparison, some tests were performed with the (D3)[25] method showing no differences in the relevant properties. To describe the Co(001) substrate, we have used a three-layer fcc Co film as in our previous works with FePc on Co(001),[16,26] with a lattice constant of 3.61 Å. For all the calculations, from the single molecule in gas phase to the dimers adsorbed on Co(001), we employed a cubic super cell of size 25.53 Å. In this way, when the cell contains the Co slab plus the MnPc dimer, a vacuum layer of about 17.5 Å is obtained between the upper MnPc and the next Co slab. The lateral distance between two MnPc molecules is about 15 Å. The density of states (DOS) curves were calculated by using 2000 points in the range of −30 to 10 eV.

RESULTS AND DISCUSSION

We have first analyzed different possible geometries for the MnPc dimer based on possible arrangements of multilayers of metal Pc molecules. We will briefly discuss these structures which are shown in Figure S1 of the Supporting Information. Starting from the α and β polymorphs, we have built the corresponding models $\alpha\times$ with a tilt angle of about 63°, the α+ with a tilt angle of 59° (Figure 1B), and the β type with a tilt angle of 43°, where the tilt angle is the angle between the line joining the two Mn atoms and a line orthogonal to the plain of the molecules. In the α+ and β configurations, the two molecules are shifted with respect to each other along an axis joining the Mn center to an isoindole N atom (N_{iso}), while in the α polymorph, the reciprocal shift occurs along a line joining the Mn center to an aza bridge N atom (N_{aza}) (see Figure 1A). The α+ configuration was previously proposed in a theoretical study of MnPc/F_{16}CoPc dimers,[8] and the magnetic properties of MnPc and CuPc in this configuration were studied by Wu et al.[9] Furthermore, this configuration was experimentally observed in a recent STM investigation of the growth of FePc multilayer films on Au(111), as the reciprocal arrangement of the molecules between the first and second FePc layers.[27] In addition to these three models, we have studied a dimer with two MnPc lying on top of each other and rotated by 45°, a structure that was for example observed as the reciprocal geometry of two CoPc in the first two layers of films of CoPc grown on a Pb(111) substrate.[17] After a geometry relaxation of all the structures, we find that α+ is the one with lowest energy, as can be seen from Table 1 with the total energies, and it is the structure the rest of this study focuses on.

To get an estimation of the magnetic coupling between the MnPc molecules in the dimers, we computed the energy difference between the ferromagnetic (FM) and the antiferromagnetic (AFM) arrangements, ΔE_{FA}, for all the structures given in Table 1. After geometry relaxation we obtain in all cases ferromagnetic coupling between the Mn

https://dx.doi.org/10.1021/acs.jpcc.0c08448
J. Phys. Chem. C 2020, 124, 27185−27193

Table 1. Total Energy Difference from the Ferromagnetic Ground State (α+) Geometry and Calculated Energy Difference between the Ferromagnetic and Antiferromagnetic Configurations (ΔE_{FA}) for All the Dimers in the Gas Phase

	structures			
	α+	β	top 45°	$\alpha\times$
ΔE (meV)	0.0	168	240	322
ΔE_{FA} (meV)	257	184	289	25

centers (corresponding to a positive value of ΔE_{FA}), but with different magnitudes in the various configurations. The top 45° dimer has the strongest coupling but has a higher total energy. In the dimers, both the α+ and the $\alpha\times$ actually have a ferromagnetic coupling according to our calculations unlike what is reported for the α polymorphs.[11,12] ΔE_{FA} is higher in the α+ and in the β dimers than in the $\alpha\times$. We attribute this to the different mechanisms that govern the magnetic coupling between the two Mn atoms which depend on their relative positions. In fact, different tilt angles in the dimers, resulting from different shifts between the planes of the two molecules, are generally expected to affect the superexchange mechanism, since the relative orientation of the molecules influences the possible overlap between different molecular orbitals. In the α+ dimer, each Mn atom is located precisely on top of a N_{iso} of the other MnPc. From the side view of Figure 1B, interestingly, it is noticeable that the MnPcs in the dimer are indeed influenced by the presence of the opposite phthalocyanine, since they are not as flat as the single molecule in gas phase (Figure 1A). The two central Mn atoms are 3.20 Å apart and slightly protruding from the plane of the molecule toward each other. For MnPc in gas phase, the computed bonding distances between the Mn and the N_{iso} atoms amount to 1.97 and 1.96 Å in the two orthogonal directions because of the D_{2h} symmetry of the molecule induced by Jahn−Teller distortions.[23,28] When the dimer is formed, the D_{2h} symmetry is lifted. The distance between the Mn and the N_{iso} that is facing the Mn of the other molecule is now 1.98 Å, slightly elongated with respect to the gas phase bond lengths, while the bonding distance with the three remaining N_{iso} is 1.96 Å.

In the Pc films, the magnetic coupling between the metal atoms is generally explained by an intermolecular superexchange interaction that connects two successive Mn centers along the chains through the N atoms of the closest molecules. The interaction depends on the overlap of the 3d orbitals of Mn with the π orbitals centered on the N atoms in the organic shell.[12]

As in the α and β phases, the relevant orbitals extending between the two molecules are the out-of-plane Mn $3d_{z^2}$ and the $3d_{\pi}$ (i.e., the $3d_{xz}$ and $3d_{yz}$) and the N_{iso} $2p_z$. One should point out that these electrons actually participate in molecular orbitals that involve also other atoms of the MnPc (C, N, and Mn). Furthermore, more than one orbital combination may contribute to the superexchange interaction, generating a more complex process than the one usually described. In a simplified scheme, the ferromagnetic superexchange coupling in the β phase is assumed to occur mainly via the overlapping of the Mn $3d_{z^2}$ with the N (π), while the antiferromagnetic coupling in the α phase via the overlapping of the Mn d_{π} with the N (π) orbitals. In the ferromagnetic α+ configuration, the atoms involved in the superexchange path form a loop that develops along the Mn centers and two of the N_{iso} atoms located on the opposite MnPc, while in the β configuration, shown in Figure S1, the superexchange path develops instead along the Mn atoms and the N_{aza} atoms. These four atoms in the α+ configuration form a rectangular loop that is highlighted in Figure 2 for three of the different structures based on the α+ dimer considered in this study and that will be discussed in the next paragraphs, namely $(MnPc)_2$ in gas phase (Figure 2A) and adsorbed on the Co substrate (Figure 2B), and $(MnPc)_2$ with a Cl axial ligand (Figure 2C). The two Mn atoms in the loop are indicated as Mn1 and Mn2 and the N_{iso} in front as N1 and N2, where the indices 1 and 2 identify the two molecules, 1 being the upper MnPc, on which the axial ligands are adsorbed, and 2 being the index of the molecule directly adsorbed on Co(001). In the bare dimer in gas phase, the superexchange loop has a regular rectangular shape with intramolecular distances between the Mn atoms and the N_{iso} of 1.98 Å and intermolecular distance between the Mn atoms and the N_{iso} of 2.74 Å. In this configuration, we obtain the highest ferromagnetic coupling, with a ΔE_{FA} value of 257 meV. The atomic distances in the four-atom loop for all the configurations studied with the respective ΔE_{FA} are reported in Table 2.

The next step was to simulate the deposition of the α+ dimer on a Co(001) surface. In our previous works regarding the adsorption of FePc on Co(001), we found a ground state corresponding to the molecule adsorbed on a *top site*, that is, with the Fe atom on top of a Co atom and with the Mn−N_{iso} main axes of the molecule oriented along the [100] crystallographic direction of the surface.[16,26] The adsorption of a single MnPc on the same surface gives analogous outcomes for structures and adsorption sites as for the FePc, as reported in Table S1. Following these results, we have placed the whole $(MnPc)_2$ dimer on the same top Co site, and the

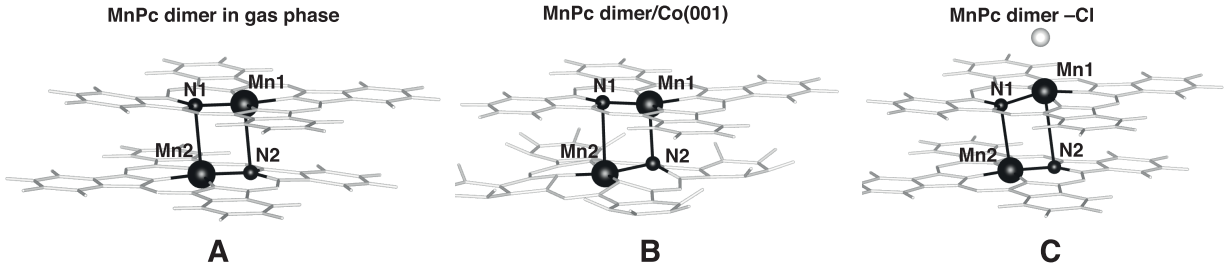

Figure 2. Four-atom loop along which the superexchange interaction Mn−N−Mn can take place between the two MnPc's in the dimer: the atoms involved in the loop are indicated as Mn1 and N1 on MnPc1, and Mn2 and N2 on MnPc2. (A) The loop in the gas phase, (B) in the chemisorbed dimer (where the surface located below the lower MnPc (MnPc2) is omitted for clarity), and (C) in the dimer with a Cl axial ligand bonded to Mn1.

https://dx.doi.org/10.1021/acs.jpcc.0c08448
J. Phys. Chem. C 2020, 124, 27185−27193

Table 2. Energy Difference between the Ferromagnetic (FM) and Antiferromagnetic (AFM) Configurations (ΔE_{FA}, meV) and Interatomic Distances (Å) within the Superexchange Loop for All the Configurations Studied

structure	ΔE_{FA}	Mn2−Mn1	Mn1−N2	N2−Mn2	Mn2−N1	N1−Mn1
$(MnPc)_2$	257	3.20	2.74	1.98	2.74	1.97
$(MnPc)_2$/Co(001)	15	3.32	2.46	2.03	2.94	1.98
H−$(MnPc)_2$	203	3.26	2.83	1.97	2.70	1.97
H−$(MnPc)_2$/Co(001)	−6	3.41	2.58	2.03	2.90	1.98
Cl−$(MnPc)_2$	18	3.62	3.03	2.01	2.97	2.00
Cl−$(MnPc)_2$/Co(001)	15	3.71	3.03	2.01	2.98	2.00

relaxed structure is displayed in Figure 1C. The chemisorption casts the dimer into a heterogeneous environment with one phthalocyanine (MnPc2) in contact with the metal and the other one (MnPc1) facing vacuum. Hence, the structural symmetry between the two molecules is lifted, with an impact on the overall geometry and properties of the dimer. A side-view inspection of the adsorbed dimer (Figure 1C) shows that MnPc2 is subject to noticeable distortions of the planar symmetry, while MnPc1 maintains a flatter geometry, akin to the gas phase molecule. The distance between the Mn atoms (Mn2 in the dimer) and the Co atom beneath is 2.43 Å for the single molecule and 2.36 Å for the adsorbed dimer, while the distance between the two Mn atoms for the adsorbed dimer is 3.32 Å, larger by 0.12 Å than in the gas phase. These distances are similar to those obtained by means of a X-rays standing wave experiment of MnPc adsorbed on Cu(001) which gave an adsorption distance of 2.240 ± 0.045 Å for the Mn to the top layer of the surface.[29] When the MnPc dimer is adsorbed on Co(001), we still obtain ferromagnetic coupling between the two molecules and between the dimer and the substrate (see Table 2). However, we find that the magnetic coupling between the two MnPc's is dramatically decreased, with ΔE_{FA} reduced to 15 meV. In practice, we find that the deposition of the dimer on the Co substrate severely weakens the magnetic coupling between the molecules. This result may imply that in a magnetic nanodevice based on a chain or on a multilayer of MnPc the first layer would not be magnetically coupled to the remaining layers. However, the magnetic moments on the Mn centers are only very little affected by the adsorption, while for similar compounds, like for CoPc on Pb(111),[30] the first molecular layer acts as a spin insulating buffer. The quenching of the coupling is reflected by the distortion of the superexchange path presented in Figure 2. In fact, the chemical bonding formed between the Mn1 center and the Co atom beneath alters the bond lengths between the N and Mn atoms reported in Table 2. In the slightly corrugated geometry of the chemisorbed MnPc2 (Figure 1) the N2 atom is lifted toward Mn1, resulting in a shorter Mn1—N2 distance (2.46 Å) and, on the other side, inducing a longer Mn2—N1 distance (2.93 Å). This can be seen from the slightly irregular loop in Figure 2B. As is also the case for the MnPc dimer with H and Cl ligands, the increase of the intermolecular Mn−N bond length between the two molecules affects the overlap of the orbitals along the loop and is correlated to the quenching of the coupling.

Experimental and theoretical studies of the axial adsorption of small molecules on several 3d metal Pc's have demonstrated how the ligands can influence the magnetic moment and spin state of the metal macrocycles.[2,31,32] Here we focus on the effect of atomic H and Cl axial ligands and on how the coupling is additionally affected by the deposition on Co(001). When a H atom is adsorbed on one side of $(MnPc)_2$, the overall geometric structure of the dimer is only marginally changed with respect to the bare dimer (Figure S2A). After geometry relaxation, the distance between Mn1 and Mn2 is 3.26 Å, which is 0.06 Å larger than in the bare dimer, and the Mn−N_{iso} distances are between 1.95 and 1.98 Å: in MnPc1, bonded to H, the Mn−N_{iso} distances are generally shorter by just about 0.01 Å. The two MnPc have ferromagnetic coupling with a ΔE_{FA} of 200 meV, which is 20% lower than in the bare dimer. In comparison to the gas phase dimer, the sides of the superexchange loop are only weakly distorted, with the Mn2−N1 distance stretched from 2.74 to 2.83 Å and the Mn1−N2 distance shortened from 2.74 to 2.70 Å (see Table 2). The deposition of the dimer on the Co(001) surface on the top site (Figure S3A) leads instead to considerable changes. We obtain a quenching of the magnetic coupling with a ΔE_{FA} of −6 meV, where the minus sign indicates an antiferromagnetic character. In this case, we find a larger distance between the Mn centers of 3.41 Å. The Mn1−N2 bond length is 2.90 Å and the N1−Mn1 bond length is 2.03 Å, thus stretching two sides of the superexchange loop with respect to the bare dimer in the gas phase.

When a Cl ligand is adsorbed on MnPc1 (Figure S2B), Mn1 is pulled toward the Cl atom, which lies 2.33 Å above it. The Mn1−Mn2 distance is increased in the presence of Cl to 3.62 Å in the gas phase and to 3.71 Å when adsorbed on the Co substrate (Figure S3B); in addition, all the bond lengths between the atoms in the superexchange loop are increased as reported in Table 2. The calculations show that in this case the Cl ligand brings about a drastic reduction of the coupling: the calculated ΔE_{FA} is 18 meV in the gas phase and 15 meV when the dimer is adsorbed on Co (see Table 2). The coupling is ferromagnetic in both cases.

The distance between the Mn1−Mn2 atoms reported in Table 2 is not a major factor in determining the strength of the magnetic interaction: for example, it only varies by 0.06 Å between $(MnPc)_2$ and H-$(MnPc)_2$, which have ΔE_{FA} differing by 20% from each other, and again it varies by 0.06 Å between H-$(MnPc)_2$ and $(MnPc)_2$ adsorbed on Co, where the coupling is reduced to 15 meV. Rather, the coupling depends mostly on a more complex interplay between the orbital overlaps along the superexchange path. Summarizing the results of Table 2 for all the systems studied, we can point out how the magnetic coupling is considerable for only two structures, namely, for the bare dimer and for the dimer with the H ligand in gas phase. In these cases, the bond lengths within the superexchange loop are very similar, with intramolecular Mn−N bond lengths between 1.97 and 1.98 Å and intermolecular Mn−N bond lengths between 2.70 and 2.83 Å. When the bare $(MnPc)_2$ is adsorbed on Co(001), ΔE_{FA} goes down to 15 meV: here the superexchange loop is distorted on one side, with the bond length Mn1−N2 increased to 2.94 Å, which is 0.2 Å more than in gas phase. When H-$(MnPc)_2$ is adsorbed

https://dx.doi.org/10.1021/acs.jpcc.0c08448
J. Phys. Chem. C 2020, 124, 27185−27193

Table 3. Magnetic Moments Obtained for Bare $(MnPc)_2$ and with H and Cl Ligands in the Gas Phase and Adsorbed on Co(001); Moments on the Mn, N, and C Atoms as Well as on the Ligand Atoms H and Cl

	magnetic moments (μ_B)						
	MnPc2			MnPc1			
configuration	Mn	C	N	Mn	C	N	ligand
monomer/dimer in gas phase							
MnPc	3.5	−0.24	−0.20				
$(MnPc)_2$	3.62	−0.24	−0.22	3.62	−0.24	−0.22	
H−$(MnPc)_2$	3.65	−0.24	−0.22	2.95	−0.27	−0.23	−0.13
Cl−$(MnPc)_2$	3.62	−0.21	−0.21	3.74	$3\cdot 10^{-3}$	−0.17	0.13
monomer/dimer on Co(001)							
MnPc/Co(001)	3.41	−0.33	−0.09				
$(MnPc)_2$/Co(001)	3.46	−0.34	−0.07	3.69	−0.24	−0.22	
H−$(MnPc)_2$/Co(001)	3.47	−0.34	−0.09	−2.80	0.22	0.20	0.11
Cl−$(MnPc)_2$/Co(001)	3.40	0.33	−0.08	3.74	0.04	−0.15	0.13

on Co, we obtain a ΔE_{FA} of −6 meV, the Mn2−N1 bond length is increased to 2.90 Å, and the Mn1−N1 bond length is increased to 2.01 Å. Finally, the dimer with Cl ligand has a ΔE_{FA} equal to 18 meV in the gas phase and 15 meV when adsorbed on the Co substrate. The Cl ligand in general induces an increase of both the intra- and intermolecular Mn−N_{iso} bond lengths, both in gas phase and on the surface.

Table 3 shows the computed magnetic moments on the Mn, C, and N atoms and on the ligands for the monomer and for all the examined configurations of the α+ dimers.

In $(MnPc)_2$ in the gas phase, in each molecule, the major part of the magnetic moment resides on the Mn atom (3.6 μ_B), while about 12% of this moment with opposite sign (−0.46 μ_B) is distributed among the N atoms and the C atoms bonded to them in the organic ring, as shown by the computed isosurface magnetization density for $(MnPc)_2$ in Figure 3A. This distribution of the magnetic moments is very similar to that of the single molecule in gas phase with 3.5 μ_B on Mn and −0.44 μ_B on the N and C atoms in the organic ring.

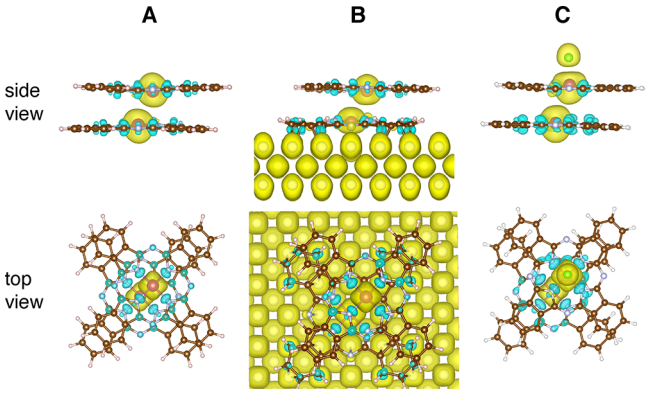

Figure 3. Side and top view of the isosurface magnetization density of (A) $(MnPc)_2$ in the gas phase, (B) $(MnPc)_2$ adsorbed on the Co(001) surface, and (C) of Cl-$(MnPc)_2$ in the gas phase. Yellow and light blue shapes indicate spin-up and -down densities, respectively.

When MnPc is adsorbed on Co(001), both as single molecule and as a dimer, we obtain a slightly smaller moment on the Mn atom directly in contact with the surface, varying between 3.41 μ_B for MnPc and 3.46 for $(MnPc)_2$, as can be seen in Table 3. At the same time, we see an increase in the moments of the C atoms in the benzene rings that bond to the Co surface by about 0.1 μ_B (see Figure 3B). On the other hand, the total moment of the N atoms decreases by about 1.1 μ_B, since here the moment in the ring is concentrated in the N_{iso} with negligible contributions from the N_{aza}. These results are similar to the variation of magnetic moments for MnPc adsorbed on Cu(001) computed with the same method by Alouani and co-workers,[29] where between gas phase and adsorption on surface, a variation in the Mn moment from 3.46 to 3.34 μ_B was found, with a change of the total C moment from −0.15 to −0.27 μ_B and a very small change of the total N moment from −0.15 to −0.14 μ_B. The small differences observed in the present work could be attributed not only to the different surfaces but also to the different adsorption sites considered in the two works, since this could affect the bonding and therefore the charge transfer of the N and C ligands to the substrate and finally their magnetic moments.

The axial ligands mainly modify the distribution of the moments in the central part of MnPc1 where they are adsorbed. In H-$(MnPc)_2$, the moment on Mn1 is 2.95 μ_B with −0.50 μ_B on the ring (about 17% of the moment on Mn1 but with opposite sign). The H ligand brings about a decrease of the moment on Mn1 accompanied by an increase of the moment on the C atoms. The Cl ligand, on the contrary, induces an increase of the magnetic moment on Mn1 to 3.74 μ_B. Now a moment of −0.17 μ_B (5% of the moment on Mn1) is located on the ring and mostly concentrated on N_{iso}, as can be seen from Figure 3C.

WhenH-$(MnPc)_2$ is adsorbed, the moment in Mn1 further decreases to −2.80 μ_B, and it goes to 0.44 μ_B on the ring. In Cl-$(MnPc)_2$ the moment stays at 3.74 μ_B on Mn1, and it is lowered to −0.11 in the ring. The antiferromagnetic coupling observed in all these cases between the central metal and the organic ring was also been observed for several metal Pc's deposited on surfaces,[29,33] while for some Pc-based 3D materials, it was found to be ferromagnetic, for example, in FePc $(CN)_2\cdot 2CHCl_3$ crystals.[34]

In addition, we have considered the magnetic interaction of the dimer to the surface, which takes place through MnPc2. We have obtained a ferromagnetic coupling of the Mn2 atom with the Co atoms as well as an antiferromagnetic coupling of the C atoms in MnPc2 to the surface. The same magnetic configuration was obtained for the single molecule and for the dimers with axial ligands. The bonding of the molecule to the surface occurs through the direct interaction of especially Mn and C atoms in the benzene rings to the underlying Co atoms, and this is coupled to variations in magnetic moment on both the MnPc and Co(001) surface. This results in a sort of

https://dx.doi.org/10.1021/acs.jpcc.0c08448
J. Phys. Chem. C 2020, 124, 27185−27193

footprint left by the molecule on the underlying surface, as can be seen in Figure 4, where the magnetic moment of the top Co

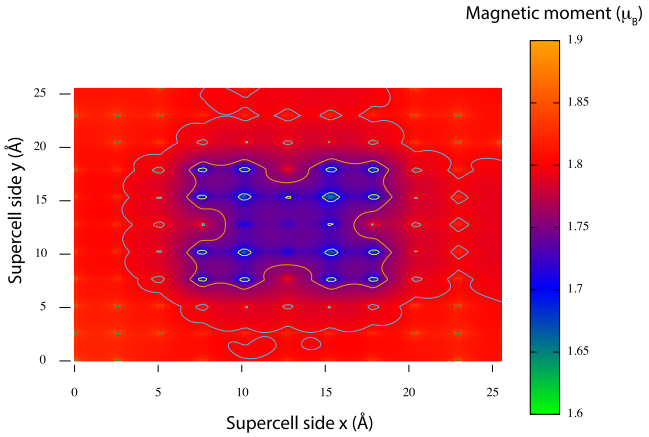

Figure 4. Magnetization density on the top Co surface layer below the adsorbed $(MnPc)_2$.

atoms on the surface are shown. A profile highlighting the position of the adsorbed molecule is also sketched. The magnetic moments of the Co atoms vary between about 1.6 and 1.9 μ_B, and the strongest variations are given by those Co atoms lying below the C atoms in the benzene rings, suggesting the decisive role played by these atoms in the bonding of MnPc to the surface. We had previously found the same type of patterning for the adsorption of FePc on the same substrate.[16]

We have finally examined the interplay between the chemical and geometrical configurations and the electronic structure of the MnPc molecules in the dimer and how this is related to the magnetic coupling. The partial density of states (pDOS) of the single molecule and of the MnPc dimer in gas phase and on Co(001) are presented in Figure 5A–C. In Figure 5A, the pDOS of the single molecule is illustrated, with the Mn 3d orbitals, $3d_{z^2}$, $3d_{\pi}$, $3d_{xy}$, and $3d_{x^2-y^2}$, and the N_{iso} $2p_z$. For the single MnPc in gas phase we obtain a ^4E_g ground state where the $3d_{z^2}$ and the $3d_{xy}$ are half occupied, and the $3d_{\pi}$ contains three electrons (see Figure 5A), in agreement with previous DFT studies[23,35] and experimental results.[36,37] MnPc's maintain the ^4E_g electronic configuration in the α+ dimer and even when they are adsorbed on Co(001) and with the axial ligands (Figure 5B,C). Because the dimer is symmetric for the two molecules, only the pDOS for one of the two is shown in Figure 5B. First of all, one can notice how the M_n $3d_{z^2}$ orbital in the dimer is split into several components of lower intensity (black lines in Figure 5). This is evident when comparing the two high-intensity $3d_{z^2}$ peaks of the single MnPc at −4.3 and 1.5 eV in Figure 5A, with the several low-intensity $3d_{z^2}$ peaks in the regions between −5.4 and −3.8 eV and between 0.8 and 2.6 eV in the gas phase dimer in Figure 5B, and is a result of the interaction between the two molecules. Also, the $3d_{\pi}$ states (gray curves) undergo some minor changes in energy position and especially in intensity, although they do not further split into several smaller components, giving a hint that the $3d\pi$ states are less involved in the hybridization between the molecules. In all the diagrams, also the partial DOS of N_{iso} $2p_z$ is plotted, for the specific N_{iso} which is located opposite to a Mn atom of the other molecule; this pDOS is very weak compared to that of the Mn 3d electrons, and its intensity is therefore multiplied by a factor 4. In $(MnPc)_2$ the N_{iso} $2p_z$ pDOS overlaps the Mn 3d orbitals in several energy intervals, like for example between −5 and −4 eV, at about 0.5 and 2 eV in Figure 5B, suggesting hybridization with the Mn 3d electrons. In this dimer as we

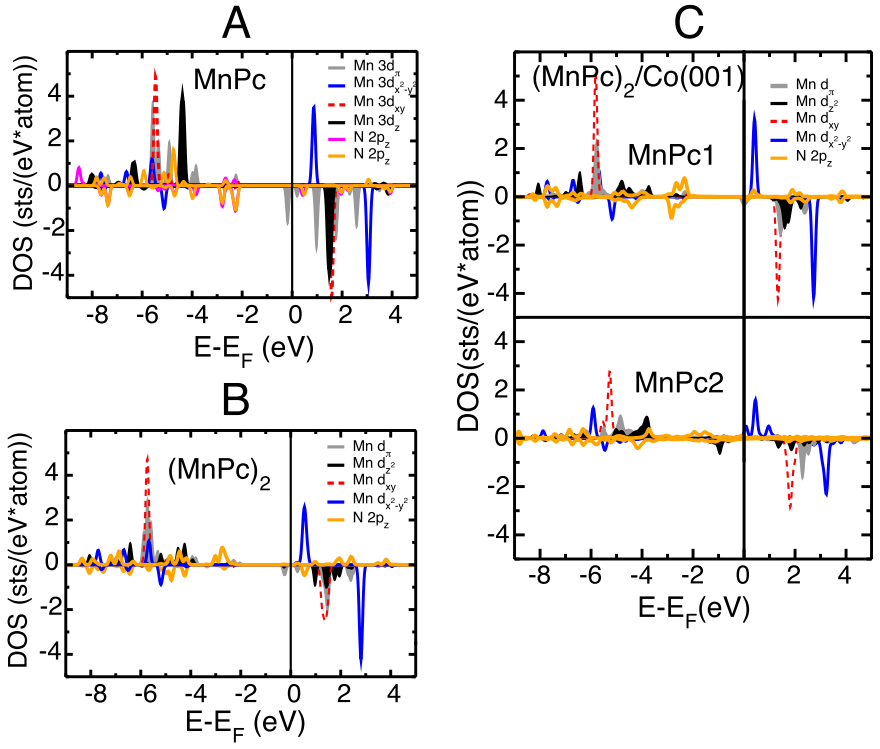

Figure 5. Partial DOS of (A) a single MnPc in gas phase, (B) of $(MnPc)_2$ in gas phase, and (C) of $(MnPc)_2$ deposited on Co(001).

https://dx.doi.org/10.1021/acs.jpcc.0c08448
J. Phys. Chem. C 2020, 124, 27185−27193

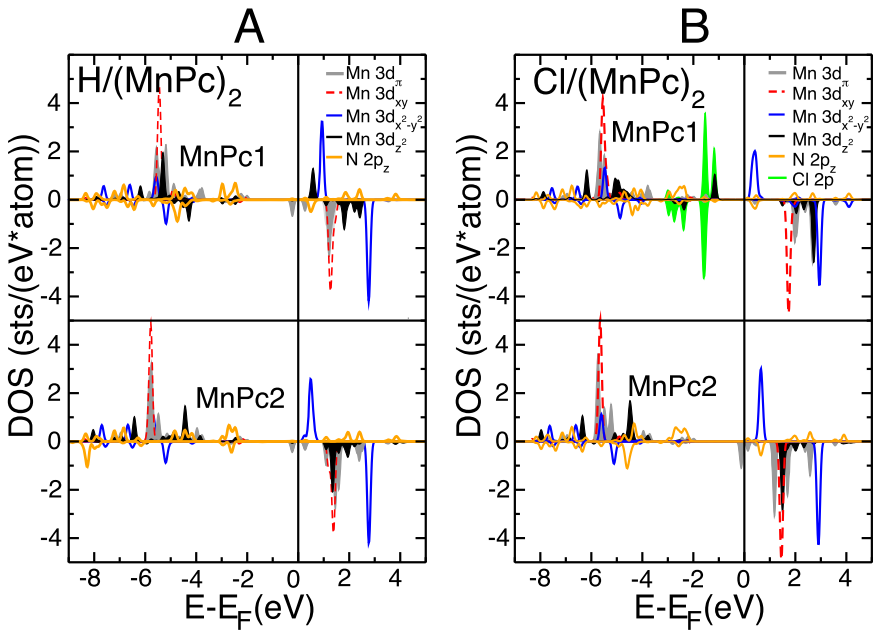

Figure 6. (A) Partial DOS of Cl−MnPc in the gas phase and (B) H−$(MnPc)_2$ in the gas phase.

have discussed before, the magnetic coupling with a ΔE_{FA} of 256 meV is strong compared to other dimer configurations.

When the MnPc dimer is adsorbed on Co(100), the lower molecule (MnPc2) is strongly bonded to the substrate. The Mn center on a top site bonds to the Co atom above through the out of plane $3d_{z^2}$ and $3d_{\pi}$ electrons. In this configuration, the MnPc is ferromagnetically coupled to the Co surface, in analogy to FePc on Co(100), as we had reported in our previous studies[16,26] and as was also found experimentally for example for the adsorbed systems FePc, CoPc, NiPc, and CuPc on Ag(100), FePc, CoPc, and CuPc on Co(001),[38] and MnPc on Co(001).[3] The pDOS curves of MnPc2 in Figure 5C show that both the *Mn* $3d_{z^2}$ and $3d_{\pi}$ electrons are strongly affected by the adsorption, with the formation of several peaks with reduced intensity. The involvement of these electrons into the bonding to the surface corresponds to a somewhat weakening of the bonding between MnPc1 and MnPc2, which could also be deduced by the flatter geometrical structure of MnPc1, and is also responsible for the drastic decrease of the magnetic coupling between the molecules with a ΔE_{FA} of 15 meV.

Figure 6A shows the pDOS of $(MnPc)_2$ with adsorbed H. Although the ferromagnetic coupling is only reduced by 20% from the bare dimer, some differences in the DOS of MnPc1 are evident. For example in the Mn1 $3d_{z^2}$ pDOS we observe a different splitting of the peaks and a new $3d_{z^2}$ feature at 0.57 eV. However, the pDOS of the MnPc2 and the N_{iso} $2p_z$ are mostly analogous to the ones of the bare dimer.

Figure 6B reports the pDOS of the dimer with the Cl ligand. In this case, a significant weakening of the magnetic coupling between the Mn centers occurs, as when the dimer is adsorbed on the Co(001). The Cl is adsorbed on MnPc1, forming chemical bonds between the M_n $3d_{z^2}$ and $3d_{\pi}$ electrons to the Cl 2p (see Figure 6B between −3 and −1 eV). These new bonds weaken the interaction between the two MnPc's significantly, which are now at 3.71 Å from each other. This effect is also visible in the pDOS of MnPc2 of Figure 5C, which resembles very closely the one of the gas phase MnPc, with distinct peaks for the M_n $3d_{z^2}$ and $3d_{\pi}$ electrons. On the other side, the pDOS of MnPc1 is highly affected by the bonding to Cl.

For all these gas phase and adsorbed systems, the pDOSs provide further evidence of the role of the M_n $3d_{z^2}$ and $3d_{\pi}$ in creating the superexchange ferromagnetic interaction between the two Mn moments, since in all cases when these orbitals are involved in other chemical bondings, the superexchange path is disturbed and the coupling gets affected.

CONCLUSIONS

To summarize, the analysis of the interplay between the reciprocal arrangement of the molecules and the magnetic interaction in the α+ dimer confirms that the magnetic coupling between the two MnPc takes principally place via superexchange interaction, exploiting one of the two paths in a loop entangling the Mn centers and two isoindole N atoms. The path is conceptually analogous to the one pointed out for the α and β bulk phase, although in the dimers only ferromagnetic coupling is obtained. In the dimer, it is possible to generate distortions in the atomic loop, for example, by chemisorption on a substrate or by adsorption of axial ligands. We have highlighted how the coupling between the molecules can be tuned by ligand adsorption, and how it can be influenced by the adsorption of the dimer on the FM Co(001). In addition, MnPc has a ferromagnetic coupling via the Mn atom to the underlying surface, but the C and N atoms have an antiferromagnetic coupling to the same.

ASSOCIATED CONTENT

Supporting Information

The Supporting Information is available free of charge at https://pubs.acs.org/doi/10.1021/acs.jpcc.0c08448.

Structures and total energies of MnPc dimers and structures and density of states of MnPc dimers with H and Cl ligands adsorbed on Co(001) (PDF)

https://dx.doi.org/10.1021/acs.jpcc.0c08448
J. Phys. Chem. C 2020, 124, 27185−27193

AUTHOR INFORMATION

Corresponding Author

Barbara Brena − *Department of Physics and Astronomy, Uppsala University, 751 20 Uppsala, Sweden;* orcid.org/0000-0003-0503-4691; Email: barbara.brena@physics.uu.se

Authors

Biplab Sanyal − *Department of Physics and Astronomy, Uppsala University, 751 20 Uppsala, Sweden*

Heike C. Herper − *Department of Physics and Astronomy, Uppsala University, 751 20 Uppsala, Sweden*

Complete contact information is available at: https://pubs.acs.org/10.1021/acs.jpcc.0c08448

Notes

The authors declare no competing financial interest.

ACKNOWLEDGMENTS

The funding from the Swedish Research Council (VR) and Carl Tryggers Foundation and eSSENCE is acknowledged as well as the Swedish National Infrastructure for Computing (SNIC) for providing computing time on the Beskow cluster at PDC, Stockholm, and at the Tetralith Cluster at NSC, Linköping. B.S. acknowledges supercomputing allocation time for the project "DYNAMAT" from PRACE.

REFERENCES

(1) Schmaus, S.; Bagrets, A.; Nahas, Y.; Yamada, T. K.; Bork, A.; Bowen, M.; Beaurepaire, E.; Evers, F.; Wulfhekel, W. Giant Magnetoresistance Through a Single Molecule. *Nat. Nanotechnol.* **2011**, *6*, 185−189.

(2) Liu, L.; Yang, K.; Jiang, Y.; Song, B.; Xiao, W.; Li, L.; Zhou, H.; Wang, Y.; Du, S.; Ouyang, M.; et al. Structure-Dependent Exchange in the Organic Magnets Cu(II)Pc and Mn(II)Pc. *Sci. Rep.* **2013**, *3*, 1210 EP.

(3) Djeghloul, F.; Ibrahim, F.; Cantoni, M.; Bowen, M.; Joly, L.; Boukari, S.; Ohresser, P.; Bertran, F.; Fèvre, P. L.; Thakur, P.; et al. Direct Observation of a Highly Spin-Polarized Organic Spinterface at Room Temperature. *Sci. Rep.* **2013**, *3*, 1272.

(4) Barraud, C.; Bouzehouane, K.; Deranlot, C.; Kim, D. J.; Rakshit, R.; Shi, S.; Arabski, J.; Bowen, M.; Beaurepaire, E.; Petroff, F.; et al. Phthalocyanine Based Molecular Spintronic Devices. *Dalton Transactions* **2016**, *45*, 16694−16699.

(5) Dediu, V.; Murgia, M.; Matacotta, F. C.; Taliani, C.; Barbanera, S. Room Temperature Spin Polarized Injection in Organic Semiconductor. *Solid State Commun.* **2002**, *122*, 181.

(6) Bagrets, A.; Schmaus, S.; Jaafar, A.; Kramczynski, D.; Yamada, T. K.; Alouani, M.; Wulfhekel, W.; Evers, F. Single Molecule Magnetoresistance with Combined Antiferromagnetic and Ferromagnetic Electrodes. *Nano Lett.* **2012**, *12*, 5131−5136.

(7) Banerjee, A.; Kundu, B.; Pal, A. J. Introducing Immobilized Metal Phthalocyanines as Spin-Injection and Detection Layers in Organic Spin-Valves: Spin-Tunneling and Spin-Transport Regimes. *Org. Electron.* **2017**, *41*, 173−178.

(8) Friedrich, R.; Lindner, S.; Hahn, T.; Loose, C.; Liebing, S.; Knupfer, M.; Kortus, J. Systematic Theoretical Investigation of the Phthalocyanine Based Dimer:$MnPc^{\delta^+}/F_{16}CoPc^{\delta^-}$. *Phys. Rev. B: Condens. Matter Mater. Phys.* **2013**, *87*, 115423.

(9) Wu, W.; Kerridge, A.; Harker, A. H.; Fisher, A. J. Structure-Dependent Exchange in the Organic Magnets Cu(II)Pc and Mn(II)Pc. *Phys. Rev. B: Condens. Matter Mater. Phys.* **2008**, *77*, 184403.

(10) Serri, M.; Wu, W.; Fleet, L. R.; Harrison, N. M.; Hirjibehedin, C. F.; Kay, C. W.; Fisher, A. J.; Aeppli, G.; Heutz, S. High-Temperature Antiferromagnetism in Molecular Semiconductor thin Films and Nanostructures. *Nat. Commun.* **2014**, *5*, 3079.

(11) Barraclough, C. G.; Martin, R. L.; Mitra, S.; Sherwood, R. C. Paramagnetic Anisotropy, Electronic Structure, and Ferromagnetism in Spin S = 32 Manganese(II) Phthalocyanine. *J. Chem. Phys.* **1970**, *53*, 1638−1642.

(12) Yamada, H.; Shimada, T.; Koma, A. Preparation and Magnetic Properties of Manganese(II) Phthalocyanine Thin Films. *J. Chem. Phys.* **1998**, *108*, 10256−10261.

(13) Sanvito, S. Molecular spintronics: The Rise of Spinterface Science. *Nat. Phys.* **2010**, *6*, 562−564.

(14) Cinchetti, M.; Dediu, V. A.; Hueso, L. E. Activating the Molecular Spinterface. *Nat. Mater.* **2017**, *16*, 507.

(15) Girovsky, J.; Nowakowski, J.; Ali, M. E.; Baljozovic, M.; Rossmann, H. R.; Nijs, T.; Aeby, E. A.; Nowakowska, S.; Siewert, D.; Srivastava, G.; et al. Long-Range Ferrimagnetic Order in a Two-Dimensional Supramolecular Kondo Lattice. *Nat. Commun.* **2017**, *8*, 15388.

(16) Klar, D.; Brena, B.; Herper, H. C.; Bhandary, S.; Weis, C.; Krumme, B.; Schmitz-Antoniak, C.; Sanyal, B.; Eriksson, O.; Wende, H. Oxygen-Tuned Magnetic Coupling of Fe-Phthalocyanine Molecules to Ferromagnetic Co Films. *Phys. Rev. B: Condens. Matter Mater. Phys.* **2013**, *88*, 224424.

(17) Chen, X.; Fu, Y.-S.; Ji, S.-H.; Zhang, T.; Cheng, P.; Ma, X.-C.; Zou, X.-L.; Duan, W.-H.; Jia, J.-F.; Xue, Q.-K. Probing Superexchange Interaction in Molecular Magnets by Spin-Flip Spectroscopy and Microscopy. *Phys. Rev. Lett.* **2008**, *101*, 197208.

(18) Kresse, G.; Furthmüller, J. Efficiency of Ab-Initio Total Energy Calculations for Metals and Semiconductors Using a Plane-Wave Basis Set. *Comput. Mater. Sci.* **1996**, *6*, 15.

(19) Perdew, J.; Burke, S.; Ernzerhof, M. Generalized Gradient Approximation Made Simple. *Phys. Rev. Lett.* **1996**, *77*, 3865.

(20) Perdew, J.; Burke, S.; Ernzerhof, M. Comment on "Generalized Gradient Approximation Made Simple. *Phys. Rev. Lett.* **1997**, *78*, 1396.

(21) Kresse, G.; Joubert, J. From Ultrasoft Pseudopotentials to the Projector Augmented-Wave Method. *Phys. Rev. B: Condens. Matter Mater. Phys.* **1999**, *59*, 1758.

(22) Dudarev, S. L.; Botton, G. A.; Savrasov, S. Y.; Humphreys, C. J.; Sutton, A. P. Electron-Energy-Loss Spectra and the Structural Stability of Nickel Oxide:An LSDA+U Study. *Phys. Rev. B: Condens. Matter Mater. Phys.* **1998**, *57*, 1505.

(23) Brumboiu, I. E.; Haldar, S.; Lüder, J.; Eriksson, O.; Herper, H.; Brena, B.; Sanyal, B. Influence of Electron Correlation on the Electronic Structure and Magnetism of Transition-Metal Phthalocyanines. *J. Chem. Theory Comput.* **2016**, *12*, 1772−1785.

(24) Grimme, S. Semiempirical GGA-type Density Functional Constructed with a Long-Range Dispersion Correction. *J. Comput. Chem.* **2006**, *27*, 1787.

(25) Grimme, S.; Antony, J.; Ehrlich, S.; Krieg, H. A consistent and Accurate ab Initio Parametrization of Density Functional Dispersion Correction (DFT-D) for the 94 Elements H-Pu. *J. Chem. Phys.* **2010**, *132*, 154104.

(26) Herper, H. C.; Bhandary, S.; Eriksson, O.; Sanyal, B.; Brena, B. Fe Phthalocyanine on Co(001): Influence of Surface Oxidation on Structural and Electronic Properties. *Phys. Rev. B: Condens. Matter Mater. Phys.* **2014**, *89*, No. 085411.

(27) Bartolomé, F.; Bunŭau, O.; García, L. M.; Natoli, C. R.; Piantek, M.; Pascual, J. I.; Schuller, I. K.; Gredig, T.; Wilhelm, F.; Rogalev, A.; et al. Molecular Tilting and Columnar Stacking of Fe Phthalocyanine Thin Films on Au(111). *J. Appl. Phys.* **2015**, *117*, 17A135.

(28) Andjelkovic, L.; Stepanovic, S.; Vlahovic, F.; Zlatar, M.; Gruden, M. Resolving the Origin of the Multimode Jahn−Teller Effect in Metallophthalocyanines. *Phys. Chem. Chem. Phys.* **2016**, *18*, 29122.

(29) Javaid, S.; Lebegue, S.; Detlefs, B.; Ibrahim, F.; Djeghloul, F.; Bowen, M.; Boukari, S.; Miyamachi, T.; Arabski, J.; Spor, D.; et al. Chemisorption of Manganese Phthalocyanine on Cu(001) Surface

Promoted by van der Waals Interactions. *Phys. Rev. B: Condens. Matter Mater. Phys.* **2013**, *87*, 155418.
(30) Wang, Y.; Zheng, X.; Yang, J. Kondo Screening and Spin Excitation in Few Layer CoPc Molecular Assembly Stacking on Pb(111) Surface: a DFT+HEOM Study. *J. Chem. Phys.* **2016**, *145*, 154301.
(31) Isvoranu, C.; Knudsen, J.; Ataman, E.; Schulte, K.; Wang, B.; Bocquet, M.-L.; Andersen, J. N.; Schnadt, J. Reversible Change of the Spin State in a Manganese Phthalocyanine by Coordination of CO Molecule. *J. Chem. Phys.* **2011**, *134*, 114711.
(32) Stróżecka, A.; Soriano, M.; Pascual, J. I.; Palacios, J. J. Reversible Change of the Spin State in a Manganese Phthalocyanine by Coordination of CO Molecule. *Phys. Rev. Lett.* **2012**, *109*, 147202.
(33) Mugarza, A.; Robles, R.; Krull, C.; Korytár, R.; Lorente, N.; Gambardella, P. Electronic and Magnetic Properties of Molecule-Metal Interfaces: Transition-Metal Phthalocyanines Adsorbed on Ag(100). *Phys. Rev. B: Condens. Matter Mater. Phys.* **2012**, *85*, 155437.
(34) Sánchez de Armas, R.; Calzado, C. J. Evaluation of the Giant Ferromagnetic π−d Interaction in Iron-Phthalocyanine Molecule. *J. Phys. Chem. A* **2018**, *122*, 1678−1690.
(35) Liao, M.-S.; Watts, J. D.; Huang, M.-J. DFT Study of Unligated and Ligated ManganeseII Porphyrins and Phthalocyanines. *Inorg. Chem.* **2005**, *44*, 1941−1949.
(36) Kroll, T.; Kraus, R.; Schönfelder, R.; Aristov, V. Y.; Molodtsova, O.; Hoffmann, P.; Knupfer, M. Transition Metal Phthalocyanines: Insight into the Electronic Structure From Soft X-Ray Spectroscopy. *J. Chem. Phys.* **2012**, *137*, No. 054306.
(37) Williamson, B. E.; VanCott, T. C.; Boyle, M. E.; Misener, G. C.; Stillman, M. J.; Schatz, P. N. Determination of the Ground State of Manganese Phthalocyanine in an Argon Matrix Using Magnetic Circular Dichroism and Absorption Spectroscopy. *J. Am. Chem. Soc.* **1992**, *114*, 2412−2419.
(38) Lach, S.; Altenhof, A.; Tarafder, K.; Schmitt, F.; Ali, M. E.; Vogel, M.; Sauther, J.; Oppeneer, P. M.; Ziegler, C. Metal−Organic Hybrid Interface States of A Ferromagnet/Organic Semiconductor Hybrid Junction as Basis For Engineering Spin Injection in Organic Spintronics. *Adv. Funct. Mater.* **2012**, *22*, 989−997.

https://dx.doi.org/10.1021/acs.jpcc.0c08448
J. Phys. Chem. C 2020, 124, 27185−27193